

***Kepler* Eclipsing Binary Stars. IV. Precise Eclipse Times for Close Binaries and Identification of Candidate Three-Body Systems**

Kyle E. Conroy

Department of Physics and Astronomy, Vanderbilt University, VU Station B 1807, Nashville, TN 37235

Department of Astrophysics and Planetary Sciences, Villanova University, 800 E Lancaster Ave, Villanova, PA 19085

Andrej Prša

Department of Astrophysics and Planetary Sciences, Villanova University, 800 E Lancaster Ave, Villanova, PA 19085

Keivan G. Stassun

Department of Physics and Astronomy, Vanderbilt University, VU Station B 1807, Nashville, TN 37235

Department of Physics, Fisk University, Nashville, TN 37208

Jerome A. Orosz

Department of Astronomy, San Diego State University, 5500 Campanile Drive, San Diego, CA 92182

Daniel C. Fabrycky

Department of Astronomy and Astrophysics, University of Chicago, 5640 S. Ellis Ave., Chicago IL 60637

William F. Welsh

Department of Astronomy, San Diego State University, 5500 Campanile Drive, San Diego, CA 92182

ABSTRACT

We present a catalog of precise eclipse times and analysis of third body signals among 1279 close binaries in the latest *Kepler* Eclipsing Binary Catalog. For these short period binaries, *Kepler*'s 30 minute exposure time causes significant smearing of light curves. In addition, common astrophysical phenomena such as chromospheric activity, as well as imperfections in the light curve detrending process, can create systematic artifacts that may produce fictitious signals in the eclipse timings. We present a method to measure precise eclipse times in the presence of distorted light curves, such as in contact and near-contact binaries which exhibit continuously changing light levels in and out of eclipse. 236 systems for which we find a timing variation signal compatible with the presence of a third body are identified. These are modeled for the light time travel effect and the basic properties of the third body are derived. This study complements Orosz et al. (2013; in prep), which focuses on eclipse timing variations of longer period binaries with flat out-of-eclipse regions. Together, these two papers provide comprehensive eclipse timings for all binaries in the *Kepler* Eclipsing Binary Catalog, as an ongoing resource freely accessible online to the community.

1. Introduction

Eclipsing binaries have historically contributed a wealth to stellar astrophysics. They have been used to determine distances, compute fundamental stellar parameters, and test stellar evolution models. The *Kepler* mission (Borucki et al. 2010; Batalha et al. 2010) and its unprecedented precise photometry of $\sim 160,000$ stars, has allowed us to create a catalog of 2605 eclipsing binaries (hereafter EBs) in the *Kepler* field (Kirk et al. 2013; in prep; Slawson et al. 2011; Prša et al. 2011). This catalog is rich in interesting objects for individual study and also presents a large sample of EBs for statistical analysis. In studying this sample, we can attempt to determine the occurrence rate of EBs, circumbinary planets, and multiple star systems.

Some theories for short-period binary star formation call for the presence of a third-body. In these scenarios, the close binary was not created *in situ*, but rather at a larger separation as a part of a multiple star system (Bonnell 2001). Tidal friction and Kozai cycles between the inner-binary and a companion can cause the inner-orbit to shrink over time (Fabrycky & Tremaine 2007), and result in a hierarchical multiple system (Reipurth & Mikkola 2012). The spectroscopy and imaging studies by Tokovinin (1997) and Tokovinin et al. (2006) have found 40% of binaries with periods less than 10 days, and 96% with periods less than 3 days, have a wide tertiary companion. The general interpretation of these findings is that the tightest binaries likely became hardened over time through interactions with the tertiary companion, and the system evolves toward an increasingly hierarchical configuration. Indeed, the SLOWPoKES study of ultra-wide binaries in the Sloan Digital Sky Survey (Dhital et al. 2010) found that the widest visual pairs with physical separations of 0.01–1 pc, in fact contain a tight binary $\sim 80\%$ of the time (Law et al. 2010), again confirming the general picture that tight binaries are nearly always accompanied by wide tertiaries and that the tightest binaries are accompanied by the widest tertiaries.

Discovery and study of these multiple systems gives new insight into the physics of EBs. Statistically, we can compare observed rates of multiple systems to theoretical models for short-period binary formation. We can also model each system individually to study the disruptive dynamical effects seen in some cases.

Kirk et al. (2013; in prep) determines ephemerides for the entire *Kepler* Eclipsing Binary Catalog. If there are no external effects, a linear ephemeris will correctly predict all eclipse times of an EB. By measuring the exact time of each eclipse for a particular binary and comparing it to the calculated time from the linear ephemeris, we can create an ETV curve (‘eclipse timing variations’; sometimes also referred to as an O-C diagram). Any trend in these timing residuals may be the result of one or more physical effects occurring in the system.

Using transit timings and eclipse timings to find exoplanets is a well-known method (Schwarz et al. 2011). Fabrycky et al. (2012), Ford et al. (2012) and Steffen et al. (2012) used transit timings to detect and study multiple planetary systems, while *Kepler* 16 (Doyle et al. 2011), 34, and 35 (Welsh et al. 2012) were validated, in part, through their eclipse timing variations. The processes that can induce ETVs, which are the focus of this paper, include the following:

- Light Time Travel Effect (LTTE): a third-body perturbing the center of mass of the binary system creates a light-time delay along the line of sight which can cause eclipses to appear earlier or later than expected.
- Non-hierarchical third-body: the presence of a third-body actually changes the period of the binary over time.
- Mass transfer: mass transfer between the components in the binary changes the period.

- Gravitational Quadrupole Coupling (Applegate effect): spin-orbit transfer of angular momentum in a close binary due to one of the stars being active produces period changes up to 10^{-5} times the binary period (Applegate 1992).
- Apical Motion: the rotation of the line of apsides causes a change in the time between primary and secondary eclipses even though the period remains unchanged (requires an eccentric orbit).
- Spurious Signals: due to spots and other effects that distort the EB light curve.

Rappaport et al. (2013) previously published a list of 39 candidate third-body *Kepler* systems using eclipse times and Gies et al. (2012) published a preliminary study on timing variations in 41 *Kepler* Eclipsing Binaries. Orosz et al. (2013; in prep) will provide eclipse times for detached binaries, and this paper provides eclipse times for close binaries. Together, these two papers will comprehensively cover all 2605 binaries in the catalog.

Kepler's essentially uninterrupted observing over a long time baseline presents the opportunity to precisely time the eclipses and detect any underlying signals due to third bodies, apical motion, dynamical interaction, etc. Due to the large number of EBs in the entire catalog, it is necessary to create an automated method for timing eclipses across the catalog. Short period and overcontact systems present a particular challenge due to spot activity and data convolution, due to a relatively long integration time.

In this paper we discuss our method for automating eclipse timings for close *Kepler* EBs in Section 2. Eclipse timings are reported for 1279 binaries in the catalog in Section 3. In Section 4, light time travel effect models for the 236 that are flagged as potential third-body candidates are also provided. We discuss our findings in Section 5 in the context of binary formation and evolution theory, and summarize our conclusions as well as information for accessing the products of our comprehensive eclipsing timing measurements in Section 6.

2. Data and Methods

2.1. Sample of Eclipsing Binaries

Kirk et al. (2013; in prep) will update the *Kepler* Eclipsing Binary Catalog, raising the count of EBs from 2165 to 2605. The database is kept up-to-date with future data and revisions at <http://keplerEBs.villanova.edu>. As changes and updates are made to the catalog, ETVs are being recomputed and updated automatically and made available in real-time through the online catalog.

Orosz et al. (2013; in prep) will provide eclipse times for binaries with flat out-of-eclipse regions, covering most of the detached binaries with periods greater than 1 day. There we locally detrend each eclipse and use a piecewise Hermite spline template to determine the time of mid-eclipse. This technique performs well on the set of detached systems but is not optimal for overcontact systems, systems with strong reflection effects or tidal distortion, or short-period binaries with only a few points in each eclipse due to *Kepler*'s 30 minute cadence. For this reason, we divide the catalog based on the morphology parameter as described in Matijević et al. (2012). This parameter is a value between 0 and 1 which describes the “detachedness” of an eclipsing binary, with 0 being completely detached and 1 being overcontact or ellipsoidal. Orosz et al. (2013; in prep) report timings for binaries with a morphology parameter less than 0.5. Our method addresses and determines eclipse times for the remainder of the *Kepler* Eclipsing Binary Catalog. The distribution of the catalog between these two methods is shown in Fig. 1, with 1279 binaries in the sample for this paper.

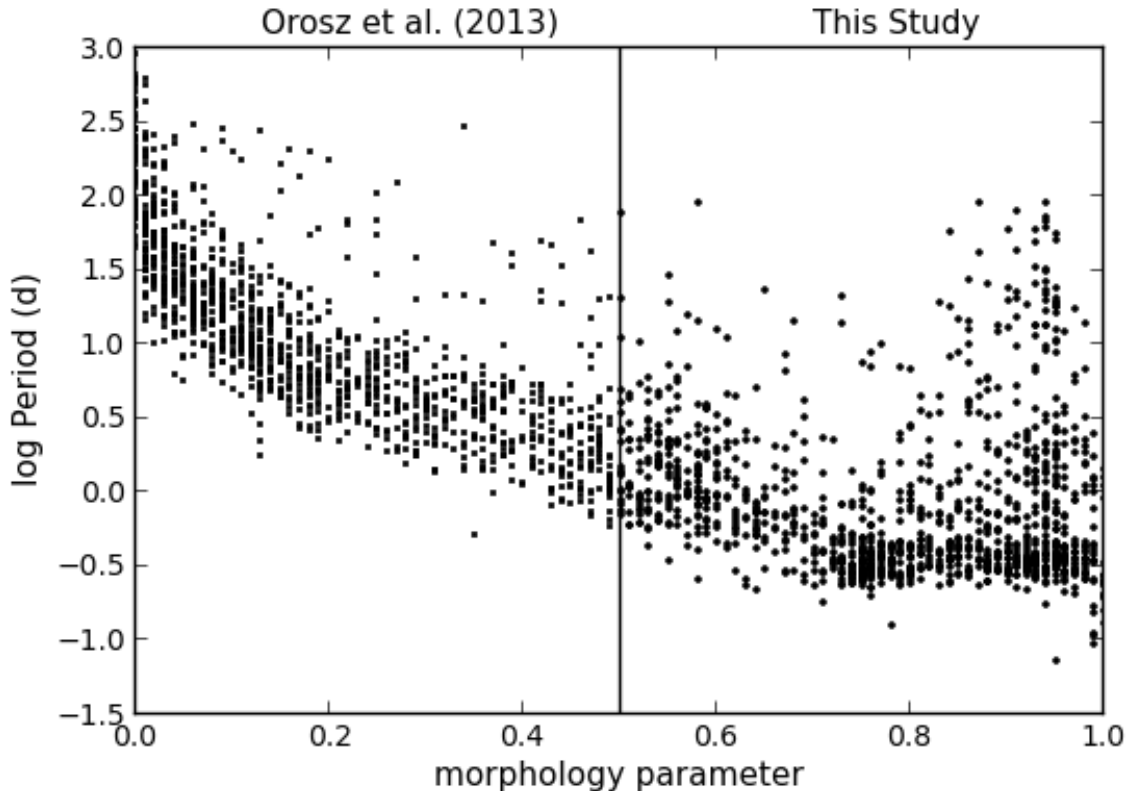


Fig. 1.— Period vs morphology parameter for the binaries in the *Kepler* Eclipsing Binary catalog. Objects included in this paper have a morphology parameter greater than 0.5.

2.2. Light Curve Preparation

We detrend and phase “SAP” (simple aperture photometry) *Kepler* data through Q16 as described in Prša et al. (2011). The upper envelope of the raw data is fit with a chain of Legendre polynomials using a sigma-clipping technique and manually setting the breaks between sections and orders of the polynomials. The data are then divided by this fit, resulting in a flat baseline. These detrended data are then phased on the linear ephemeris as reported in Kirk et al. (2013; in prep), and used as input into the ETV code, described below.

2.3. Measuring Eclipse Times

We fit a polynomial chain to the phased light curve data as described in Prša et al. (2008). This analytic function is a chain of four polynomials that is continuous, but not necessarily differentiable, at knots which were optimized to find the best overall solution. This function does not represent a physical model, but rather analytically describes the mean phased shape of the binary light curve, an example of which can be seen in Fig. 2.

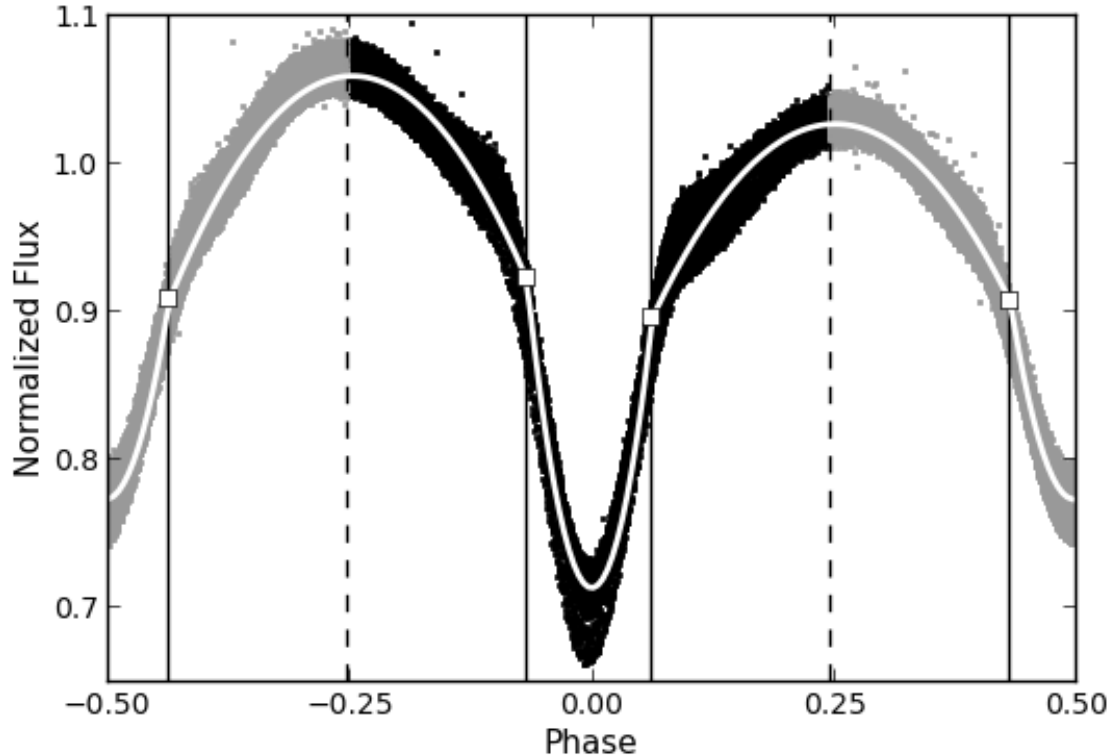


Fig. 2.— Typical polyfit and eclipse bounds for a semi-detached binary. The polyfit knots are indicated with the squares and solid vertical lines, with the polyfit drawn in white over the data. Data considered as part of the primary eclipse are shown in black while those belonging to the secondary eclipse are shown in gray. The eclipse bounds are set at the arithmetic bisector of the adjacent knots and are shown with dashed vertical lines.

We then take this analytical representation and, using a combination of heuristic and bisection approaches, determine the horizontal shift required to minimize the χ^2 (cost function) for each individual eclipse as shown in Fig. 3. In order to minimize the effect due to spots or imperfect detrending, a vertical shift is first determined using linear least squares for each eclipse and is applied before computing cost functions for horizontal shifts. The cost function is initially sampled at 20 evenly-spaced phase shifts between -0.05 and 0.05 phase. The minimum of this sampling is then used as the center of the bisection algorithm to quickly find the local minimum of the cost function. The resulting χ^2 values are unusually large because the errors on the *Kepler* data are only formal and do not include any absolute calibration effect (Jenkins et al. 2010). Therefore, for each eclipse, we normalize the entire cost function such that the minimum cost is set to $N - p - 1$, where N is the number of data points used for that eclipse and p is the degrees of freedom, which we take to be 1. This reduced cost function is then used to compute 1-sigma errors on each timing to correspond to the $\Delta\chi^2 = 1$ contour.

For the shortest binaries in the catalog, however, the long-cadence data result in significant phase-smearing and limits our method to a very minimal number of points per cycle to determine a fit. If there

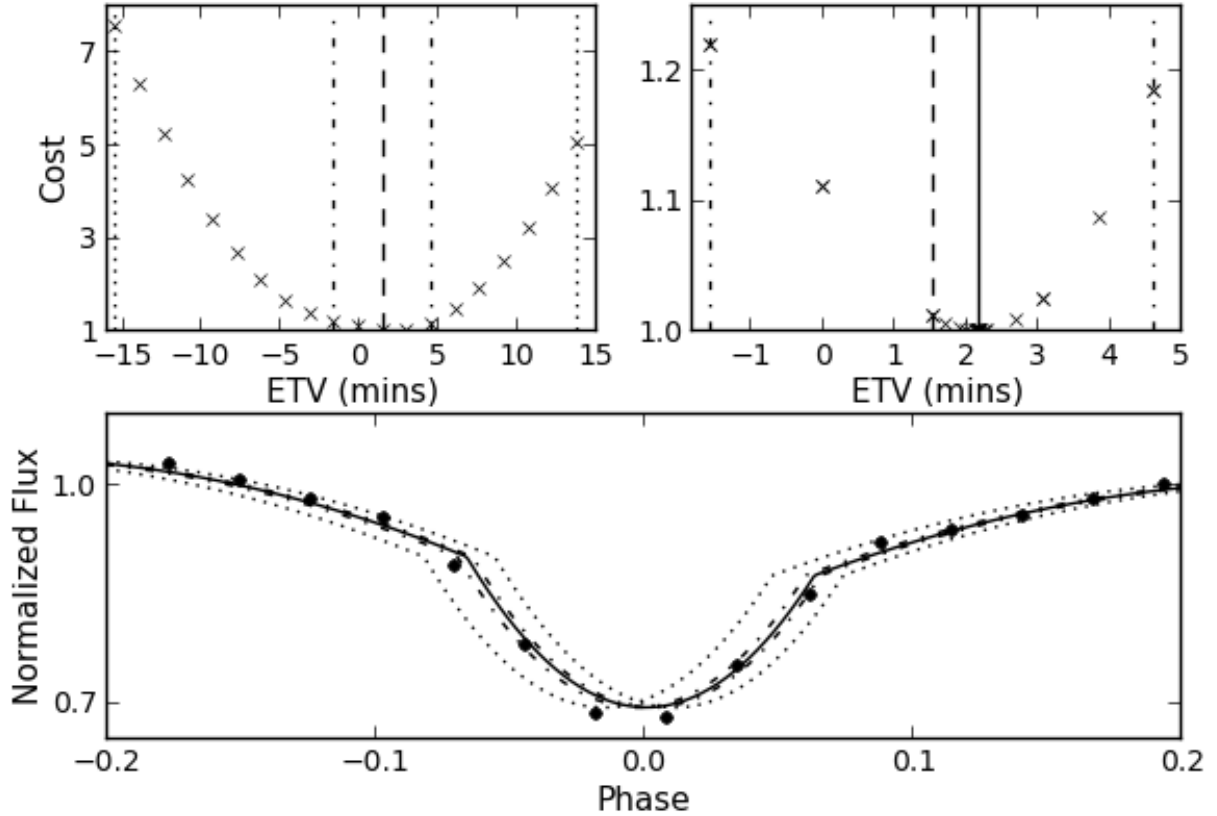


Fig. 3.— Reduced cost function (χ^2) values, shown as x’s, are computed heuristically (top-left) for 20 evenly-spaced phase-shifts within 0.05 phase, shown by the dotted lines in all panels. The best fit of these is shown with the dashed line in the top-left panel. A bisection approach (top-right) is then applied in the area surrounding this estimate, as shown by the dot-dashed lines. This results in a final minimum at the phase shift denoted by the solid line. The bottom plot shows the data for a single eclipse along with the polyfits for the respective shifts noted above.

were to be a third-body, the signal would likely be buried in the noise induced by these factors. For this reason, we include as many data points as possible in each eclipse timing. Each data point is considered to belong to an eclipse if its phase as determined by the initial linear ephemeris is within bounds. We initially set these bounds to be the mid-point between polyfit knots in the out-of-eclipse region as shown in Fig. 2. To improve results for particular objects being studied individually, changing these bounds to use the knots (instead of the mid-points) can sometimes lower the systematics in the signal. For any given eclipse, if the region between these bounds is not fully sampled or does not have at least 3 data points, then timings are not computed for that eclipse. Eclipse timings are then compared to the values expected from the linear ephemeris as reported by Kirk et al. (2013; in prep) to compute the residuals and test for the presence of an ETV signal.

2.4. Dealing with Sources of Spurious ETV Signals

Due to a typically small number of points per eclipse, our timings are sensitive to various imperfections in the data processing, affecting the measured eclipse time and potentially introducing noise and/or fictitious signals in the ETV signal. Instrumental or astrophysical pulsations on top of the binary signal can change the shape of a single eclipse which can mimic a timing variation. The detrending process attempts to remove these additional signals, but is not perfect, struggles at removing signals that happen during eclipse, and can also introduce spurious signals. Also, all polyfits in the current version of the catalog use chains of four second-order polynomials, which does not always result in the ideal fit and can leave slight phase-dependent residuals. For the purpose of pipeline processing, we limit ourselves to second order polynomials, but note that, for special cases and in-depth studies, higher precision timings can be obtained by increasing the order of the fit. Until all polyfits are updated to a higher order in the future, we will use the second-order fits and manually run ETV signals with a higher order for any individual ETV signals that warrant further study. In the cases when a binary has a period that is near-commensurate to *Kepler*’s 29.44 minute cadence, the period and cadence may beat, which results in a separate spurious signal. Any combination of these effects can cause issues in determining true and precise eclipse times when dealing with only a few data points.

Fig. 4 demonstrates how the cost function for the phase shift is affected by the vertical discrepancy in the out-of-eclipse region, creating a fictitious signal in which the ETVs of the primary and secondary eclipse are in anti-phase. The left of Fig. 4 plots four different eclipses, showing that over time the data in the out-of-eclipse region can be higher on either the right or the left. When measuring timings for the primary and secondary separately, the cost function will artificially be minimized by “pulling” the analytic function towards the region with lower flux. Since this will affect the primary and secondary in the opposite direction, we can mitigate for this effect by also running the fit over the entire phase. This effectively averages out the anti-phase effect in the primary and secondary eclipses, projecting the real ETV signal of the entire system. Fig. 5 shows two cases where the anti-phase signal was removed, clearly showing whether there is a presence of any underlying ETV signal. These signals that show a “random walk” nature are discussed by Tran et al. (2013).

Unfortunately, since there is no rigorous way to discriminate between true and fictitious anti-phase signals, this process would also hide a physical ETV signal such as apsidal motion. Since we are dealing with short-period binaries, most of these orbits will be quite circular so we do not expect to be able to detect any systems with apsidal motion anyway.

2.5. Short-Cadence Data

If a binary has short-cadence data available, they are usually limited to a short time baseline. Since we are generally looking for long period trends in the ETV signal, we measure timings from the full long cadence dataset. We also run timings on any available short cadence data in case some signal can be detected.

A few short period binaries in the catalog that appear to be overcontact or ellipsoidal variables could actually be detached systems whose light curves are convolved by *Kepler*’s 30 minute long cadence exposure. Since these systems are less prone to timing noise due to spots or mass transfer than true overcontact systems, the phase smearing and limited data points per eclipse are the main issues preventing us from recovering any ETV signal. For this reason, short cadence data were requested and obtained via Director’s Discretionary Time for 31 short-period detached EBs in the catalog without previous short-cadence observations in the hope of detecting third-body ETV signatures which were not visible in the long-cadence data. Unfortunately,

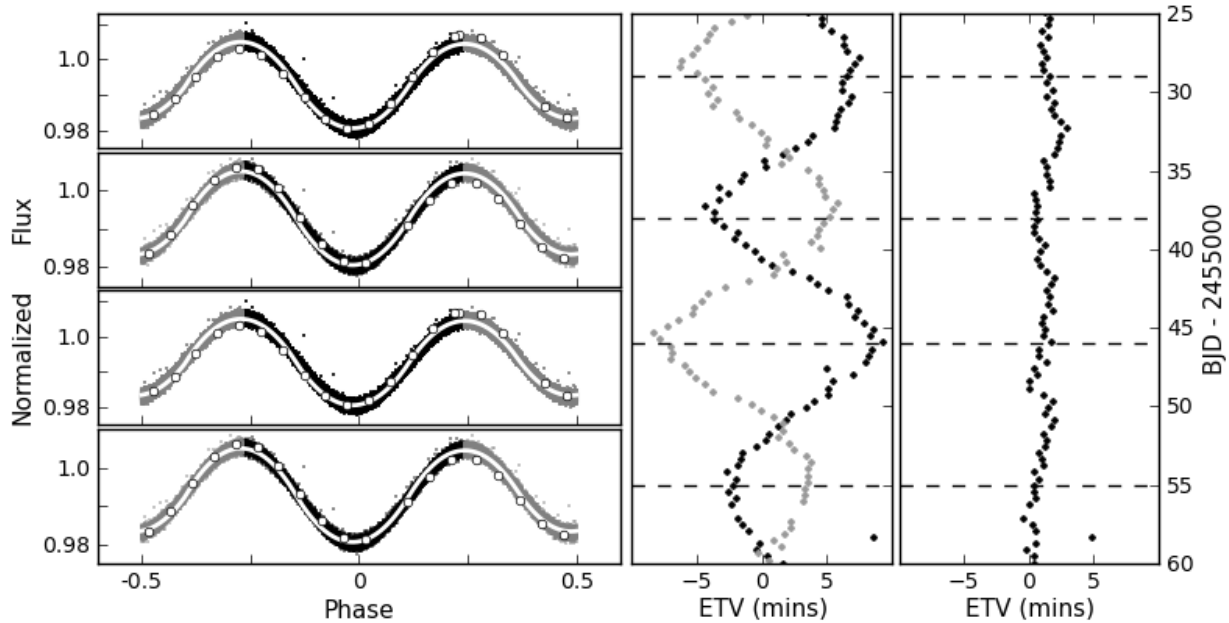


Fig. 4.— Determining eclipse timings using both eclipses will cancel the anti-phase effect and reveal any underlying signal. The plots on the left show a phased light curve with primary eclipse data in black and secondary in gray with the analytic ‘polyfit’ in white. These four plots highlight the data during individual cycles (shown in white on the left) at four different times noted in the ETV plots with the dashed line, showing the presence of spots. The plots on the right show the ETV as measured at for primary and secondary eclipses separately (middle) and full phase (right).

none seem to exhibit any significant ETVs.

Eclipse times are computed for all available short-cadence data, but due to the longer baseline, long-cadence timings are used for detection and fitting of potential third-body orbits.

3. Results

3.1. Precise Eclipse Times

Eclipse timing variations on the individual eclipses and the entire phase have been run for all objects with a morphology parameter greater (less detached) than 0.5 in the latest *Kepler* Eclipsing Binary Catalog. Our method requires at least 3 data points per timing, which allows us to get primary and secondary eclipse timings individually for long cadence data of binaries with periods as short as 3 hours and full phase timings for binaries as short as 1.5 hours. We are able to determine timings for any binary with short cadence data, but since short cadence data availability is sparse and generally not for the whole length of the mission, short cadence ETVs are determined separately.

Plots and data for detrended light curves and eclipse times for the entire sample are available as a part of the *Kepler* Eclipsing Binary online catalog at <http://keplerEBs.villanova.edu>. An excerpt of the eclipse times is shown in Table 1. With the third version of the catalog being released shortly, the database will be

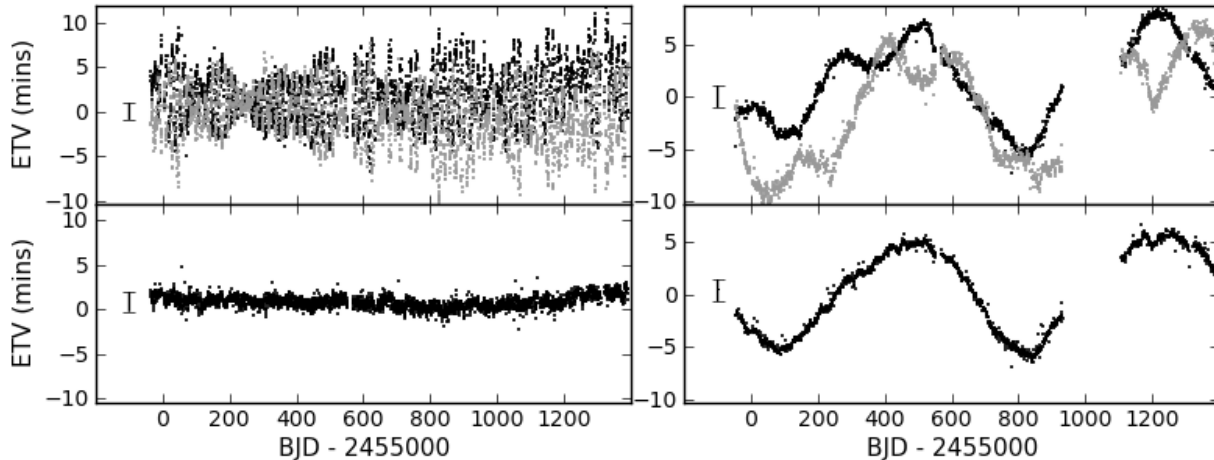


Fig. 5.— ETVs for KIC 6880727 (left) and 4451148 (right) determined for primary and secondary eclipses separately (top) and together (bottom). KIC 6880727 (left) shows an example with no underlying signal under the antiphase “noise”, while KIC 4451148 (right) shows a possible underlying third-body signal. Typical errors for ETV measurements are shown to the left of the data.

updated as new data become available and ephemerides are further refined. This ETV code is incorporated into the pipeline: as objects are updated or added, their ETVs are recomputed and updated in real-time.

As ETVs are computed, the ephemerides in the catalog are refined by fitting a linear fit through the entire-phase timings and adjusting the values as necessary to get a “flat” trend. For any ETV with a long-term sinusoidal trend, this could introduce systematics depending on the part of the sine curve observed and used to fit the linear trend. In particular, for very long ETV signals (of the order of 1000 days and more), the measured orbital period of the binary will be anomalous because the variation cannot be accounted for from available data.

3.2. Causes of an ETV Signal

All ETV measurements were examined by eye for the presence of any interesting signal, discarding any that seem to be spurious based on their individual primary and secondary eclipse timings. We do not expect to see evidence of apsidal motion in many of our targets due to their short periods and, consequently, circular orbits. We also do not expect to be able to detect any signals due to gravitational quadrupole coupling. This mechanism is able to create period changes with amplitudes on the order of 10^{-5} times the period of the binary, meaning a maximum of 3.5 seconds for a binary with a period of 4 days, falling well within our noise limits.

ETV signals that are sinusoidal in nature or show any sign of curvature are flagged and fit for both a third-body signal and a parabolic mass transfer model. For the cases where we only see a sign of curvature and not a full cycle, we could either be seeing a section in a long period third body signal or mass transfer. To determine whether we consider the signal as a candidate third body or mass transfer, we compare the

two models using the Bayesian Information Criterion (Schwarz 1978):

$$BIC = n \ln \left(\frac{1}{n} \sum (x_i - \hat{x}_i)^2 \right) + k \ln n \quad (1)$$

where x_i are the data, \hat{x}_i the model, n the number of data points, and k is the number of parameters used in the fit. In the case of the eccentric LTTE model $k = 6$, for the circular LTTE model $k = 4$, and for the mass transfer model $k = 3$. The better fit, as determined by the lower BIC value, then determines whether we consider the signal as a candidate third body or mass transfer.

3.3. ETVs with Parabolic Signals

Thirty-one ETV signals were better fit by a parabola than an LTTE orbit, and are possibly caused by mass transfer or the Applegate effect instead of the presence of a third body (Hilditch 2001). A selection of these signals are shown in Fig. 6, all KICs are listed in Table 6, all of which are available on the online catalog.

3.4. ETVs with Third-Body Signals

236 binaries ($\sim 20\%$ of the sample) were flagged as candidate third bodies. The results of the model fits are reported in Table 3 with a selection plotted in Fig. 7. Based on the fitted period, we then divided these third body candidates into three sections. The first group contains third body signals with periods less than 700 days, such that there are at least two full cycles of the signal present in data through Q16. These systems have the highest confidence and are most likely due to the presence of a tertiary component. The second group contains signals with periods between 700 and 1400 days, such that there is at least one full cycle present. The last group contains signals with periods longer than 1400 days. Often these detections merely show some sign of curvature in the ETV signal and so a full sinusoidal signal cannot yet be confirmed. For this reason the fits generally have large errors and many of these may not even be true triple systems, particularly the signals on the closest binaries which are more likely to be due to mass transfer.

Gies et al. (2012) presented an initial study of eclipse timings in 41 *Kepler* binaries. Of their entire sample of 41 binaries, 40 are still in the *Kepler* EB Catalog (KIC 4678873 has since been removed from the catalog as a false positive), 32 fall under the scope of this paper (have a morphology less detached than 0.5), and 9 appear in our list of third-body signals. They identified 14 out of their original 41 as candidate third-body systems, with others being identified as likely caused by starspots, pulsations, and apsidal motion. Of their 14 candidate third-body systems, all 14 are still in the *Kepler* EB Catalog, 12 fall under the scope of this paper, and 9 appear in our list of third-body signals. Those that appear in both lists are noted in Table 4. Binaries that they list as candidate third-body systems, but we do not, either show significant noise or would be very long period LTTE orbits.

Rappaport et al. (2013) recently reported 39 triple-star *Kepler* binaries due to ETV signatures. Of these 39, 21 fall under the scope of this paper, 19 of which also appear in our list of third-body signals, with the other two determined to be unlikely caused by a third-body due to their very short periods and notable spot activity. The detections that overlap both of these studies are also noted in Table 3. In most cases, the model fits from both studies are consistent. In general, due to our treatment of the full *Kepler* dataset now available, tertiary parameters should now be more precise and longer period third body signals are now

more apparent. Any disagreement is likely due to a slightly differ inner-binary ephemeris or the addition of the physical delay in their models (discussed further below).

4. Analysis of Third Body Signals

4.1. Light Time Travel Effect Analysis

Borkovits et al. (2011) presents analytic functions for the light time travel effect (LTTE) component of the ETV residual signal. Using the same form as Rappaport et al. (2013), the timings can be expressed by

$$ETV_{LTTE} = A_{LTTE} \left[(1 - e_3^2)^{1/2} \sin E_3(t) \cos \omega_3 + (\cos E_3(t) - e_3) \sin \omega_3 \right] \quad (2)$$

where

$$E_3(t) = M_3(t) + e_3 \sin E_3(t) \quad (3)$$

$$M_3(t) = (t - t_0) \frac{2\pi}{P_3} \quad (4)$$

$$A_{LTTE} = \frac{G^{1/3}}{c(2\pi)^{2/3}} \left[\frac{m_3}{m_{123}^{2/3}} \sin i_3 \right] P_3^{2/3} \quad (5)$$

and t_0 is a time offset, m_3 is the mass of the third body, m_{123} is the mass of the entire system, and P_3 , i_3 , e_3 , ω_3 , $E_3(t)$, and $M_3(t)$ are the period, inclination, eccentricity, argument of periastron, eccentric anomaly, and mean anomaly of the third body orbit, respectively.

This expression was then used to fit all ETVs flagged as potential third body signals. The period was first estimated using Lomb-Scargle periodogram and used as input into a series of Levenberg-Marquardt fits, each using a different starting guess for eccentricity. The fit with the lowest chi-squared was then kept and the errors estimated from the covariance matrix. If the final fit had an eccentricity consistent with 0, then e_3 was set to 0, ω_3 to $\pi/2$, and the fitting was redone with circular constraints to get appropriate error estimates on the remaining parameters.

This gives values and estimated errors for P_3 , e_3 , and A_{LTTE} (Table 4). A sample of some of these ETV signals and their respective fits can be seen in Fig. 7, with fits for all candidate third body signals available in the online version of the *Kepler* EB Catalog. We can only provide estimate periods for the sample of ETV signals with less than one full cycle in the data. Even these periods can be significantly biased based on the section of the cycle that is in the observed baseline and should be treated with reservation. These very long period cases are provided separately at the end of Table 4

4.2. Physical Delay

Rappaport et al. (2013) included physical delays in their models of 39 *Kepler* binaries with possible third-body ETVs, sometimes contributing largely to the overall model. This dynamical effect occurs when the presence of a third body changes the period of the inner binary. Fig. 8 shows the distribution in their targets and the overlapping targets of the ratio of the amplitude of the physical delay compared to the total amplitude in the ETV signal. 21 of their targets overlap with ours, but due to the short-period inner-binary, the physical delay rarely contributes significantly to these model. From their results, it seems that the LTTE

effect dominates over the physical delay for binaries with periods less than 3 days, which covers the vast majority of our targets.

4.3. Objects with Tertiary Eclipses

For some of these binaries with LTTE signals, tertiary eclipses have also been found that confirm the presence and third body period, and significantly constrain the inclination of the third body. Any binary which was identified to have a possible third body due to its ETV signal and also has a detected tertiary eclipse is noted as such in Table 4.

KIC 2856960, for instance, has an inner-binary period of 0.259 days with an ETV signal resulting in a LTTE fit with a period of 205.5 ± 0.1 days. This period is consistent with the previously determined period for the tertiary events of 204.25 days (Fig. 9). This is also consistent with the LTTE period of 205 ± 2 days reported by Lee et al. (2013), and the tertiary event period of 204.2 days by Armstrong et al. (2012).

In the case of KIC 2835289 (Fig. 10), we have only observed one potential tertiary event in Q9. Without at least three consecutive events, we cannot rigorously confirm that the eclipse is a third-body as opposed to a blended eclipsing binary. However, the eclipse seems to show the eclipse of both stars in the inner-binary and ETV signal shows a possible long-term third body orbit suggesting a period of approximately 800 days. If this proves to be a true third body, then *Kepler* just missed an event before the beginning of the mission and may have observed another event in Q17, which has yet to be processed.

KIC 6543674 also shows a single tertiary eclipse in Q2. A second tertiary eclipse was missed during a break in the *Kepler* data, but we were able to observe an additional tertiary event from the ground, giving a third body period of ~ 1100 days (Thackeray-Lacko et al. 2013). In this case, we do not have a full orbit of the ETV signal and the LTTE model period is quite uncertain.

4.4. Objects with Depth Variations

Nine binaries that show third-body ETV signals (KIC 3936357, 4069063, 5310387, 6629588, 7375612, 8122124, 8758716, 10014830, and 10855535) also show constant changes in their eclipse depths (Fig. 11), which could either be caused by a change in inclination or apsidal motion perhaps induced by the third body. We plan to follow these up later with full photodynamical models.

4.5. Potential Fourth Body Signals

It is also possible that some of these ETVs could be composed of multiple signals. KIC 5310387, 6144827, 8145477, 11612091, and 11825204, for example, may have both an LTTE and quadratic component or two LTTE signals as is shown in the residuals in Fig. 12. In general, the stronger signal is fitted and noted.

5. Discussion

In this study we find a third body rate of $\sim 20\%$ in our sample of close binaries, nearly all of which have inner binary periods shorter than 3 days (Fig. 13). This is much lower than the third body rate of 96%

found by the previous studies mentioned. However, our identification of tertiary companions is certainly a lower limit for several reasons.

First, our ability to detect a third body is very sensitive to both inclination and mass of the third body, such that low-mass tertiaries and/or tertiaries whose orbital planes are highly inclined relative to the inner binary orbital plane do not present detectable LTTE effects. Of our total sample of 1279 binaries, 3 (< 1%) show an LTTE orbit and visible tertiary eclipses. 111 ($\sim 10\%$) have LTTE orbits with periods shorter than the span of our photometric data but do not show tertiary eclipses, suggesting that the eclipses fell in a gap in the data or the orbits are not well enough aligned to show eclipses. Thus there is evidence from these examples that in a few percent of cases we are indeed missing true third bodies because of inclination non-alignments. 94 ($\sim 7\%$) have LTTE orbits with periods longer than the photometric baseline. In these cases we do not have well constrained periods and our chances of detecting a tertiary eclipse are slim.

A second reason that our determination of the third-body occurrence is likely a lower limit is that the very close binaries that comprise our sample here generally present more noise in the ETV signal, which could easily bury a weak LTTE signal. We have employed a method that minimizes false positives due to spurious ETV signals, and thus necessarily have eliminated some potentially true LTTE signals.

Third, and perhaps most important, the limited timespan of the currently available *Kepler* data (~ 1400 days) significantly restricts us to detect third bodies with orbital periods comparable to or shorter than 1400 days. Relative to the full span of tertiary separations found in previous works (Tokovinin 1997; Tokovinin et al. 2006; Dhital et al. 2010; Law et al. 2010), with separations as large as ~ 1 pc, we are at present sampling only the relatively closest tertiary companions. Indeed, Tokovinin et al. (2006) found among tight binaries that the rate of third bodies with orbital periods less than ~ 3 years (comparable to our limit based on the duration of the available *Kepler* data) is $15\% \pm 3\%$. Thus our finding of a third-body occurrence rate with a period less than 1400 days of $\sim 10\%$ is compatible with the expected rate, though it appears we are likely still missing a fraction of some systems for the reasons already mentioned.

The distribution of periods of potential third body orbits is also shown in Fig. 13. We can clearly see a falloff in detection past the current length of the *Kepler* mission of ~ 1400 days, as expected. However, for third-body periods shorter than ~ 1400 days, for which our detectability is relatively good, the occurrence rate does appear to increase toward longer third-body periods, consistent with the period distribution of third bodies among tight binaries found by Tokovinin et al. (2006). Furthermore, we find that the triples on the widest orbits are found around the shortest period binaries, which is consistent with models that tighten the inner binary orbit through the presence, and gradual widening, of a companion.

6. Summary and Conclusions

We presented our technique for computing precise eclipse timings for 1279 close eclipsing binaries in the *Kepler* Eclipsing Binary Catalog. These precise eclipse timings are complemented by the eclipse timings to be reported by Orosz et al. (2013; in prep) for longer period, detached EBs. For the EBs whose timings are reported here, our method has been developed specifically to deal with the challenge of constantly changing light levels arising from spots and other phenomena that distort the light curves and could cause spurious eclipse timing variation (ETV) signals.

EBs with ETV signals suggesting the possible presence of a third body have been identified and have been fit with a LTTE orbit model in order to determine the likely parameters of the third bodies. In

the current sample of 1279 close EBs, we have identified 236 that likely have tertiary companions. The parameters of these fits are also available online and are updated as new data become available.

Our measured occurrence rate of $\sim 10\%$ of close binaries with tertiary companions with periods up to ~ 1400 days (limited by the current timespan of *Kepler* data), appears to be broadly consistent with the expectation that $15 \pm 3\%$ of close binaries will have tertiaries of such periods (Tokovinin et al. 2006). Indeed, we already find in our data that the periods of third bodies rise among the tightest binaries, consistent with previous work that has found a very high rate of third bodies in very wide orbits around the tightest binaries, presumably the result of dynamical tightening of inner binaries through widening of the tertiary.

Eclipse timings for all EBs are updated in real-time and are freely available as a community resource at <http://keplerEBs.villanova.edu>.

Acknowledgements

We thank Nathan De Lee and Phil Cargile for helpful discussions and Darin Ragozzine, Eric Ford, and Joshua Pepper for their feedback.

This project is supported through the *Kepler* Participating Scientist Award NSR303065. KEC and KGS acknowledge support from NASA ADAP grant NNX12AE22G. JAO and WFW gratefully acknowledge support from the NSF via grant AST-1109928, and also NASA via the *Kepler* PSP grant NNX12AD23G.

Kepler was selected as the 10th mission of the Discovery Program. Funding for this mission is provided by NASA, Science Mission Directorate.

REFERENCES

- Applegate, J. H. 1992, *ApJ*, 385, 621
- Armstrong, D., Pollacco, D., Watson, C. A., et al. 2012, *A&A*, 545, L4
- Batalha, N. M., Borucki, W. J., Koch, D. G., et al. 2010, *ApJ*, 713, L109
- Bonnell, I. A. 2001, *The Formation of Binary Stars*, 200, 23
- Borkovits, T., Csizmadia, S., Forgács-Dajka, E., & Hegedüs, T. 2011, *A&A*, 528, A53
- Borucki, W. J., Koch, D., Basri, G., et al. 2010, *Science*, 327, 977
- Dhital, S., West, A. A., Stassun, K. G., & Bochanski, J. J. 2010, *AJ*, 139, 2566
- Doyle, L. R., Carter, J. A., Fabrycky, D. C., et al. 2011, *Science*, 333, 1602
- Fabrycky, D. C., Ford, E. B., Steffen, J. H., et al. 2012, *ApJ*, 750, 114
- Fabrycky, D., & Tremaine, S. 2007, *ApJ*, 669, 1298
- Ford, E. B., Ragozzine, D., Rowe, J. F., et al. 2012, *ApJ*, 756, 185
- Gies, D. R., Williams, S. J., Matson, R. A., et al. 2012, *AJ*, 143, 137
- Hilditch, R. W. 2001, *An Introduction to Close Binary Stars*, by R. W. Hilditch, pp. 392. ISBN 0521241065. Cambridge, UK: Cambridge University Press, March 2001.
- Jenkins, J. M., Caldwell, D. A., Chandrasekaran, H., et al. 2010, *ApJ*, 713, L120
- Law, N. M., Dhital, S., Kraus, A., Stassun, K. G., & West, A. A. 2010, *ApJ*, 720, 1727
- Lee, J. W., Kim, S.-L., Lee, C.-U., et al. 2013, *ApJ*, 763, 74
- Kirk et. al 2013 (in preparation)
- Matijević, G., Prša, A., Orosz, J. A., et al. 2012, *AJ*, 143, 123
- Orosz et al. 2013 (in preparation)
- Prša, A., Batalha, N., Slawson, R. W., et al. 2011, *AJ*, 141, 83
- Prša, A., Guinan, E. F., Devinney, E. J., et al. 2008, *ApJ*, 687, 542
- Rappaport, S., Deck, K., Levine, A., et al. 2013, arXiv:1302.0563
- Reipurth, B., & Mikkola, S. 2012, *Nature*, 492, 221
- Schwarz, G. 1978. *The Annals of Statistics*, 6, 461
- Schwarz, R., Haghighipour, N., Eggl, S., Pilat-Lohinger, E., & Funk, B. 2011, *MNRAS*, 414, 2763
- Slawson, R. W., Prša, A., Welsh, W. F., et al. 2011, *AJ*, 142, 160
- Steffen, J. H., Ford, E. B., Rowe, J. F., et al. 2012, *ApJ*, 756, 186

Thackeray-Lacko, B., Hill, M., Orosz, J. A., et al. 2013, American Astronomical Society Meeting Abstracts, 221, #142.09

Tokovinin, A. A. 1997, Astronomy Letters, 23, 727

Tokovinin, A., Thomas, S., Sterzik, M., & Udry, S. 2006, A&A, 450, 681

Tran, K., Levine, A., Rappaport, S., et al. 2013, ApJ, 774, 81

Welsh, W. F., Orosz, J. A., Carter, J. A., et al. 2012, Nature, 481, 475

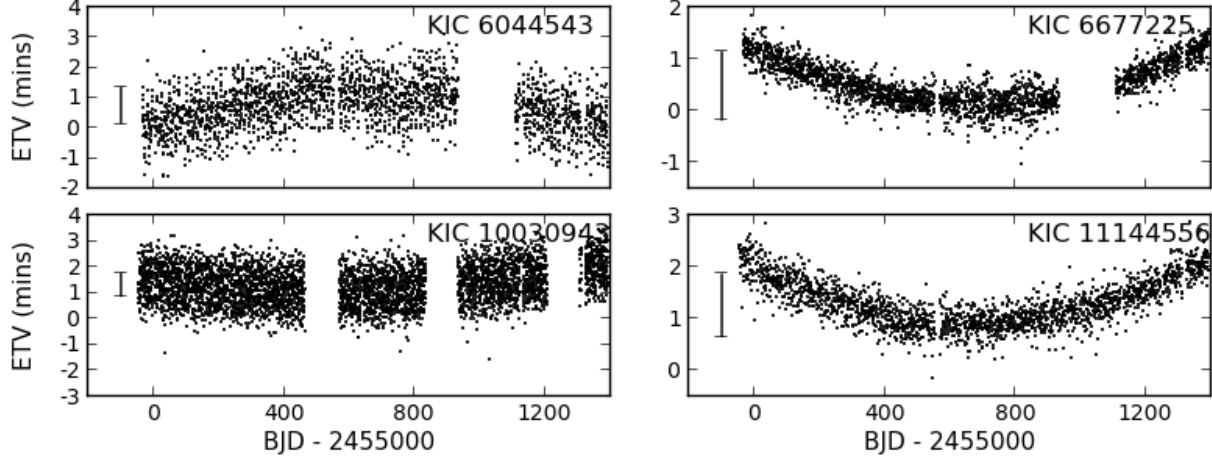


Fig. 6.— A selection of ETV signals that are better fit by a quadratic ephemeris than a LTTE fit.

Table 1. Eclipse Timing Variations

KIC	BJD_{ecl}	ETV (s)	$\sigma(ETV)$ (s)	Eclipse
1433410	56107.275	-6.307	39.658	primary
1433410	56107.275	-4.493	20.390	entire
1433410	56107.416	-47.606	40.954	secondary
1433410	56107.558	-10.541	18.835	entire
1433410	56107.558	21.341	30.499	primary
1433980	55740.148	-443.232	143.078	secondary
1433980	55740.944	-283.392	70.502	primary
1433980	55740.944	-170.899	69.552	entire
1433980	55741.741	-161.482	90.634	secondary
1433980	55742.537	-248.659	61.776	primary

Note. — The full electronic table is available in the online version.

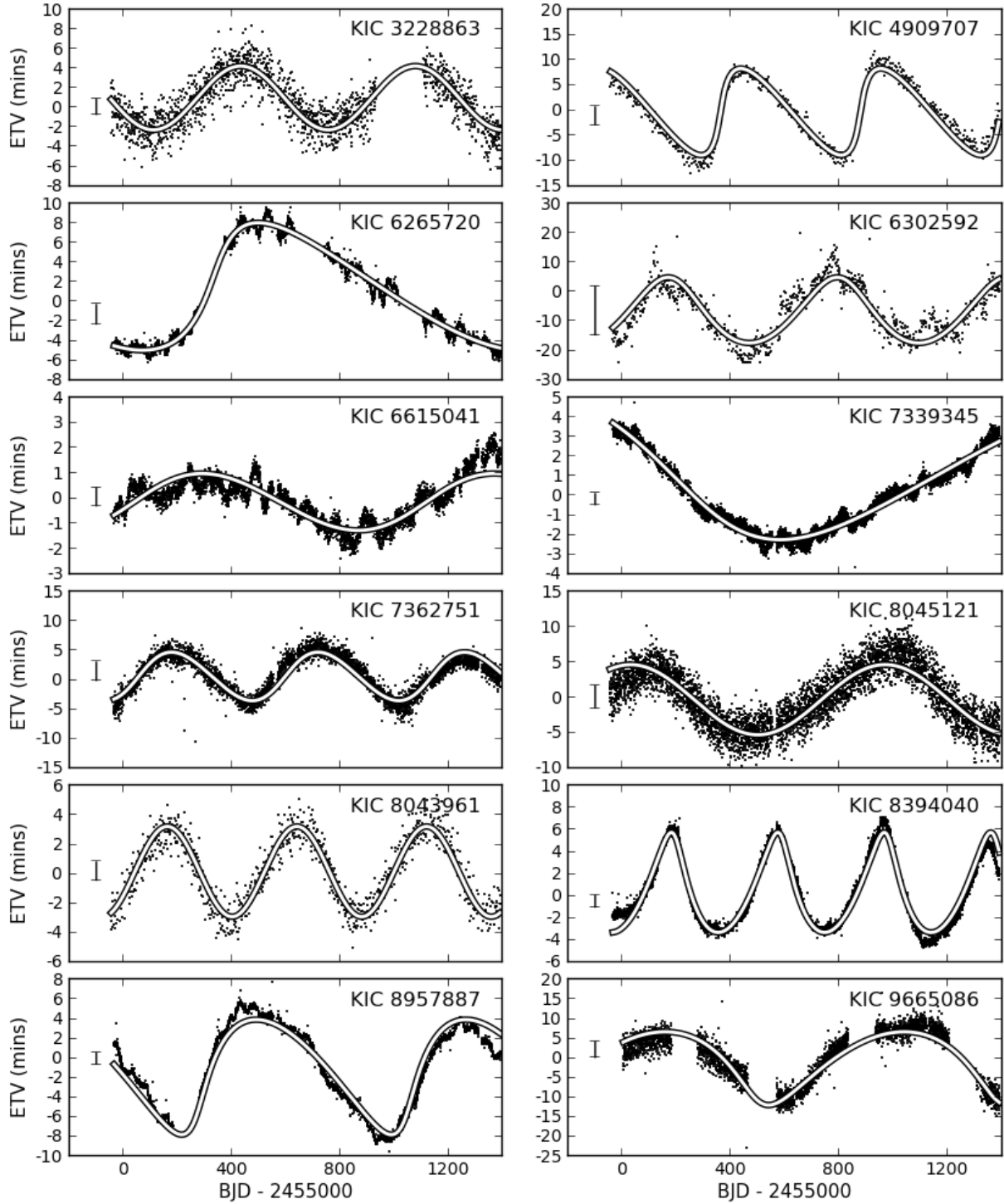


Fig. 7.— Gallery of select ETV signals found in close binaries with LTTE fits. These are KIC 3228863, 4909707, 6265720, 6302592, 6615041, 7339345, 7362751, 8045121, 8043961, 8394040, 8957887, and 9665086. Typical errors for ETV measurements are shown to the left of the data.

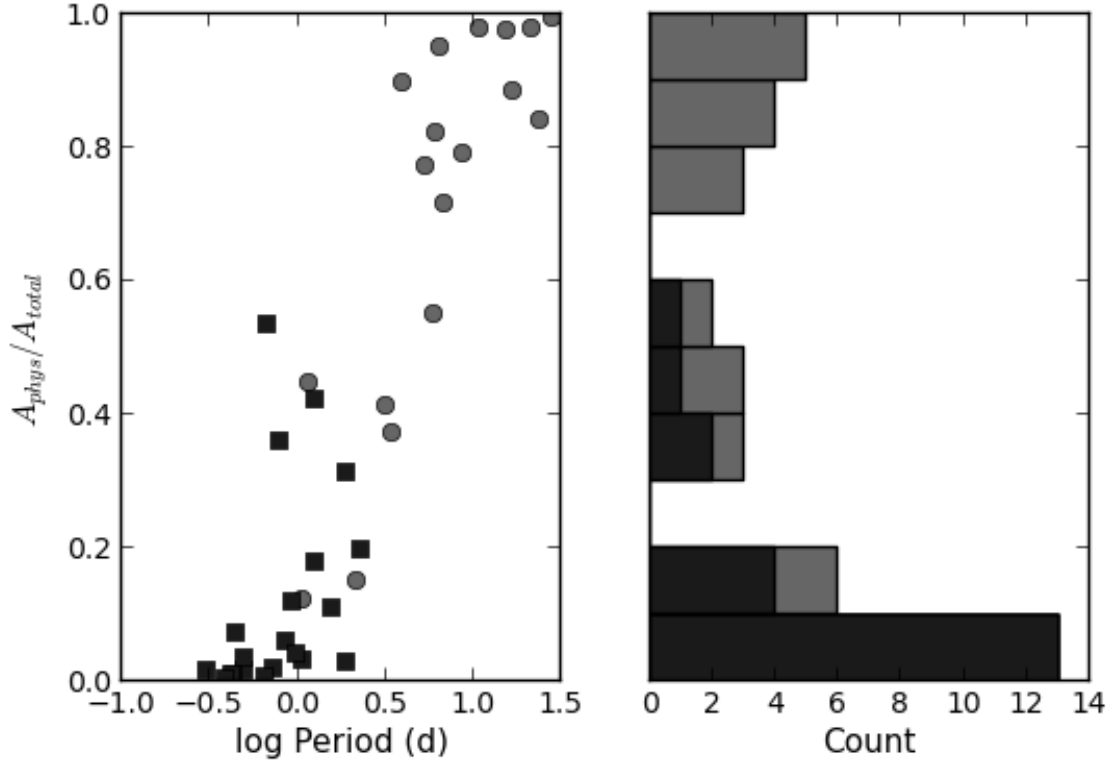


Fig. 8.— Distribution of the contribution to the total ETV amplitude due to physical effects (Rappaport et al. 2013) . The left plot shows this distribution versus the log of the period of the inner-binary, with the systems that overlap with this paper as dark squares, and those that do not as lighter circles. The right panel shows a histogram of these contributions, with the overlapped systems highlighted with the darker shade.

Table 2. ETVs with Parabolic Signals

KIC	KIC	KIC
2305372	3104113	3765708
4074532	4851217	4853067
5020034	5471619	5770860
5792093	6044064	6044543
6066379	6213131	6314173
6464285	6677225	7696778
7938468	7938870	8758161
9087918	9402652	9840412
9934052	10030943	10292413
10736223	11097678	11144556
11924311

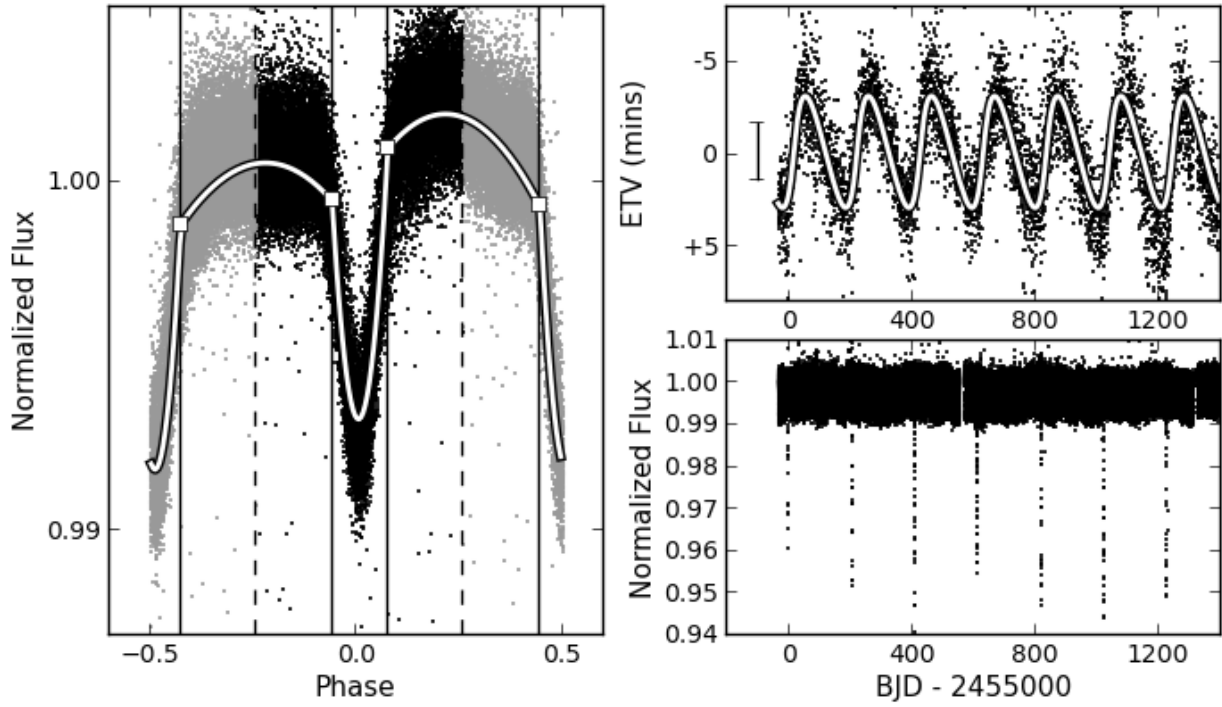


Fig. 9.— A triple eclipsing star KIC 2856960. Left: the detrended light curve phased at the inner period of 0.26-d. The white line is the polyfit function, and white rectangles are the knots. Dashed lines delimit the phase space of the primary and secondary eclipse; these are used separately to obtain primary and secondary ETVs. Upper right: the measured ETVs (black points) and the best light-time travel fit (white line), yielding the outer period of 205.5 days. Lower right: the detrended light curve, with the tertiary eclipses clearly visible.

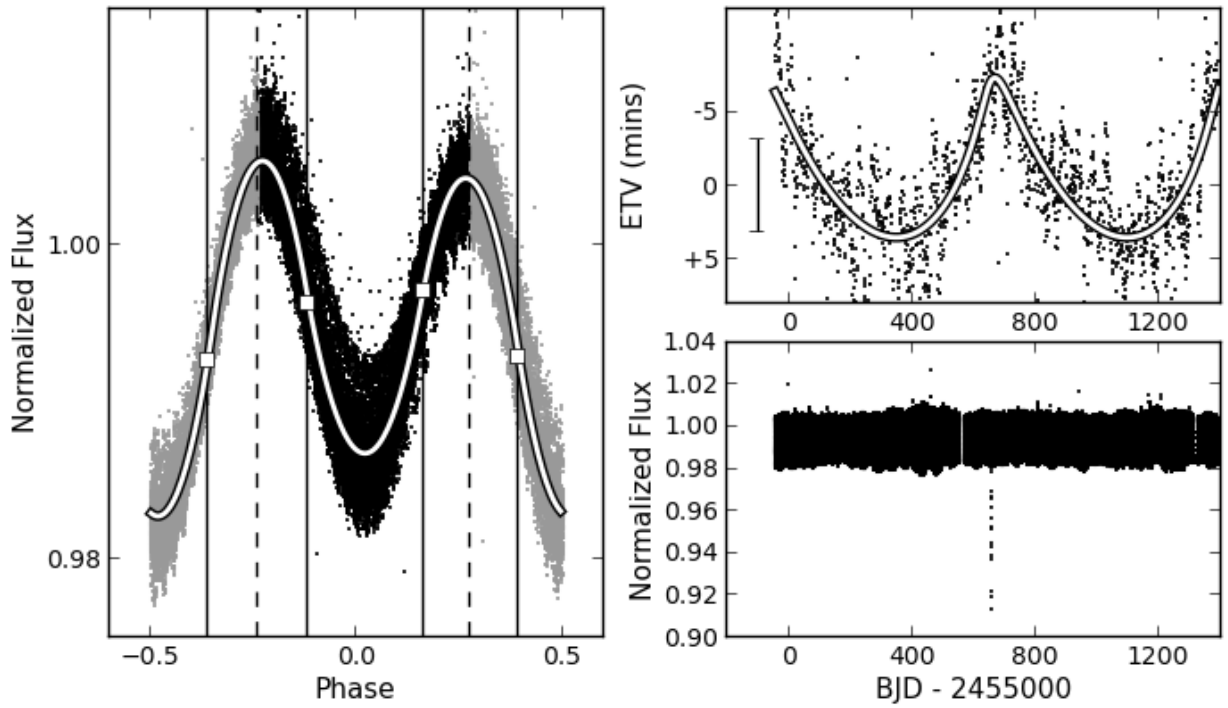


Fig. 10.— KIC 2835289 is an ellipsoidal variable with a period of 0.857 days. We can see one tertiary eclipse in the light curve and the ETV signal can put an additional constraint on the expected period of a potential third-body.

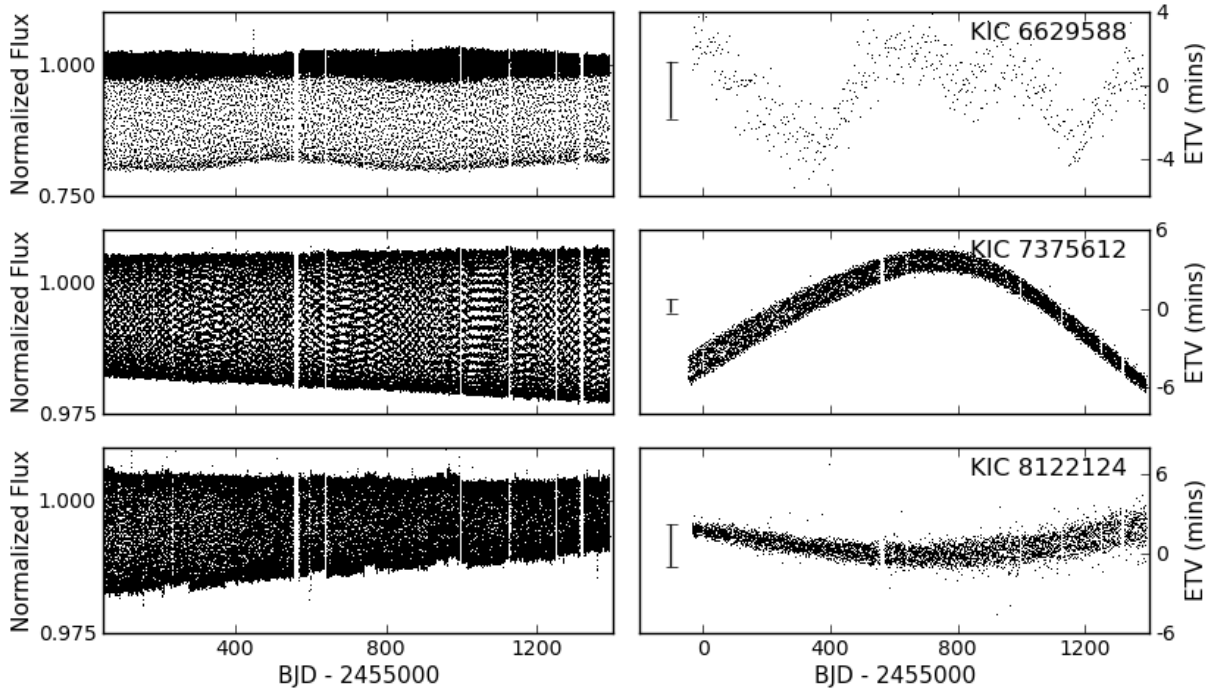


Fig. 11.— KIC 3936357, 4069063, 5310387, 6629588, 7375612, 8122124, 8758716, 10014830, and 10855535 all show ETVs that suggest a possible third body and eclipse depth variations. In some of these cases the template polyfit causes systematics in the timings, and could be improved by creating new templates for each quarter.

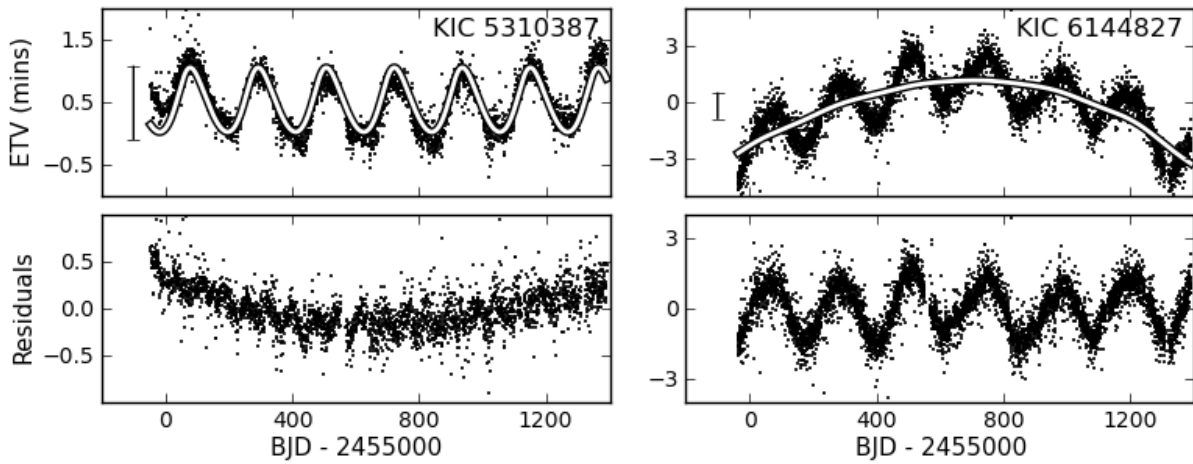


Fig. 12.— KIC 5310387 and 6144827 are among several ETV signals with residuals that suggest another parabolic or LTTE signal, possibly indicating the presence of a fourth body.

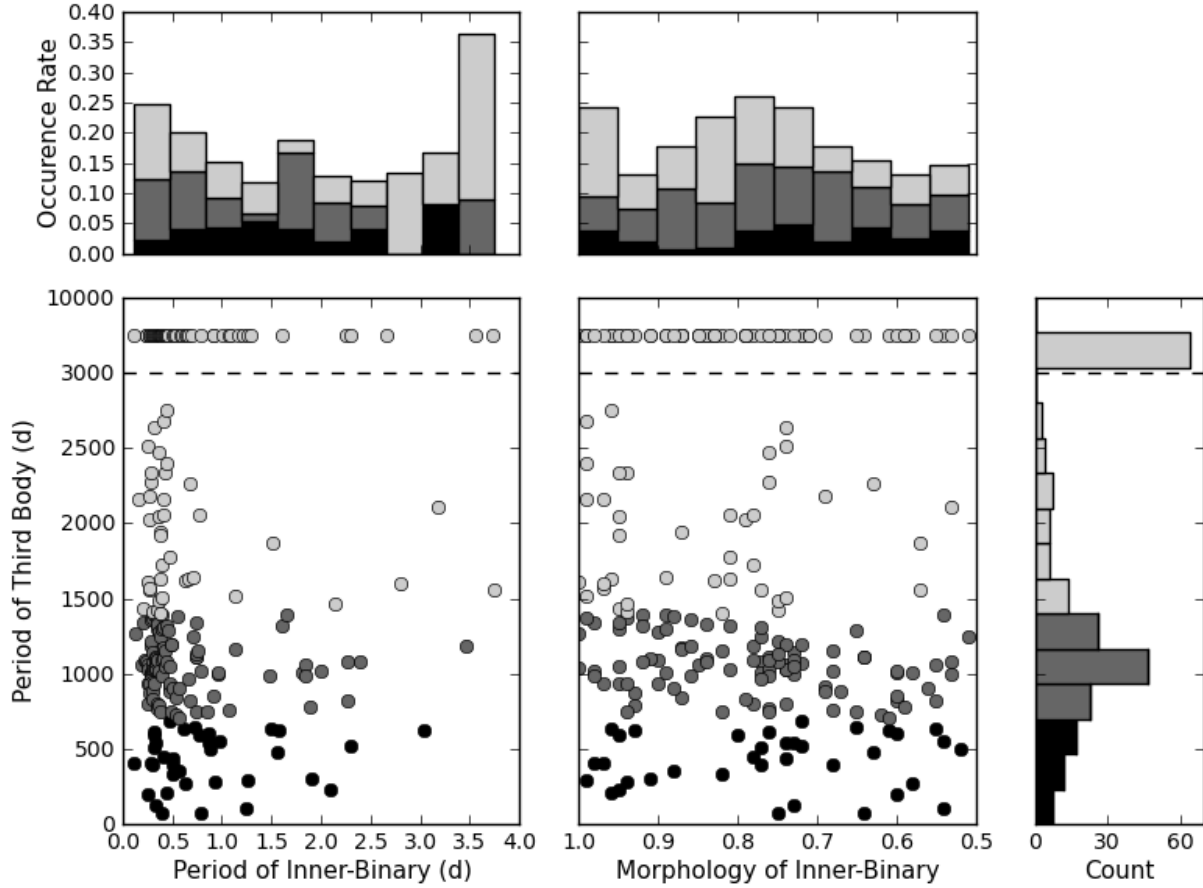


Fig. 13.— Distribution of period of potential third body companions versus the inner-binary period (left) and morphology (right). Third body periods greater than 3000 days are all placed in the final bin despite their modeled periods. The different colors represent the three different samples of binaries represented in Table 4, determined by the period of the potential third body. The top histograms show the occurrence rate of candidate third bodies for each bin in period or morphology, and the histogram on the right shows the number of third body candidates at each period.

Table 3. ETVs crossmatched with Rappaport et al. (2013)

KIC	$P_{3,R}$ (d)	P_3 (d)	$e_{3,R}$	e_3	$A_{LTTE,R}(s)$	$A_{LTTE}(s)$
3228863	668.4	644.1 ± 15.7	0.08{0.06,0.12}	0.000 ± 0.003	189{187,194}	195 ± 3
4647652	753.5	755.2 ± 44.3	0.35{0.10,0.44}	0.244 ± 0.003	228{183,274}	239 ± 9
4909707	505.3	516.1 ± 16.1	0.54{0.31,0.66}	0.686 ± 0.006	493{378,627}	707 ± 14
5128972	447.8	438.7 ± 1.9	0.33{0.25,0.41}	0.323 ± 0.002	259{244,271}	256 ± 1
5264818	296.3	299.7 ± 107.5	0.37{0.13,0.53}	0.421 ± 0.306	145{107,196}	178 ± 42
5310387	214.2	214.3 ± 0.3	0.53{0.34,0.61}	0.250 ± 0.004	31{ 27, 37}	31 ± 1
5376552	334.5	331.1 ± 0.8	0.40{0.35,0.45}	0.000 ± 0.002	94{ 91, 98}	87 ± 1
6370665	285.9	283.2 ± 20.9	0.22{0.07,0.33}	0.136 ± 0.085	67{ 61, 74}	66 ± 3
6531485	48.3	...	0.44{0.33,0.63}	...	72{ 31,109}	...
7690843	74.3	74.1 ± 0.1	0.25{0.08,0.42}	0.233 ± 0.021	71{ 51, 91}	81 ± 1
8043961	476.7	478.0 ± 10.4	0.25{0.14,0.33}	0.000 ± 0.005	194{179,213}	184 ± 2
8192840	803.9	1045.9 ± 185.0	0.63{0.52,0.70}	0.616 ± 0.002	208{187,223}	260 ± 30
8386865	293	293.9 ± 2.8	0.38{0.27,0.48}	0.493 ± 0.013	171{156,210}	197 ± 1
8394040	394.8	392.6 ± 0.8	0.61{0.50,0.67}	0.467 ± 0.001	369{345,391}	278 ± 1
8904448	548.1	538.8 ± 59.9	0.59{0.50,0.66}	0.577 ± 0.016	171{158,192}	166 ± 12
9451096	106.7	106.8 ± 0.1	0.24{0.10,0.36}	0.091 ± 0.033	90{ 59,144}	93 ± 1
9722737	443.9	451.3 ± 3.7	0.22{0.16,0.27}	0.152 ± 0.003	230{225,236}	225 ± 1
9912977	753.7	780.4 ± 95.2	0.31{0.16,0.39}	0.504 ± 0.008	105{ 94,117}	96 ± 7
10226388	934.9	965.3 ± 183.8	0.32{0.24,0.39}	0.041 ± 0.007	465{434,493}	457 ± 58
10991989	554.2	554.8 ± 64.1	0.30{0.21,0.37}	0.000 ± 0.018	256{239,274}	232 ± 17
11042923	839	984.4 ± 63.9	0.17{0.09,0.25}	0.258 ± 0.002	223{213,230}	276 ± 11

Note. — $P_{3,R}$, $e_{3,R}$, and $A_{LTTE,R}$ are the period, eccentricity, and amplitude as reported by Rappaport et al. (2013)

Table 4. ETVs with Potential Third-Body Signals

KIC	morph _{bin}	P_{bin} (d)	P_3 (d)	e_3	$A_{LTTE}(s)$
2856960 ⁵	0.60	0.259	204.5 ± 0.1	0.447 ± 0.001	202 ± 1
3228863 ¹	0.65	0.731	644.1 ± 15.7	0.000 ± 0.003	195 ± 3
3245776	0.96	1.492	636.3 ± 70.6	0.587 ± 0.021	136 ± 10
3641446	0.95	2.100	228.6 ± 1.0	0.000 ± 0.010	85 ± 1
4037163	0.58	0.635	267.0 ± 8.1	0.349 ± 0.009	77 ± 1
4909707 ¹	0.72	2.302	516.1 ± 16.1	0.686 ± 0.006	707 ± 14
5128972 ¹	0.74	0.505	438.7 ± 1.9	0.323 ± 0.002	256 ± 1
5264818 ¹	0.91	1.905	299.7 ± 107.5	0.421 ± 0.306	178 ± 42
5310387 ^{1 4}	0.96	0.442	214.3 ± 0.3	0.250 ± 0.004	31 ± 1
5376552 ¹	0.82	0.504	331.1 ± 0.8	0.000 ± 0.002	87 ± 1
5459373	0.97	0.287	411.5 ± 1.2	0.372 ± 0.002	228 ± 1
5560831	0.60	0.868	609.0 ± 149.2	0.093 ± 0.010	58 ± 9
6302592	0.93	1.578	623.6 ± 42.9	0.211 ± 0.009	671 ± 30
6370665 ¹	0.94	0.932	283.2 ± 20.9	0.136 ± 0.085	66 ± 3
7362751	0.73	0.338	540.3 ± 3.4	0.162 ± 0.001	250 ± 1
7657914	0.72	0.475	689.9 ± 295.1	0.405 ± 0.025	30 ± 8
7685689	0.77	0.325	507.3 ± 6.2	0.176 ± 0.002	183 ± 1
7690843 ¹	0.64	0.786	74.1 ± 0.1	0.233 ± 0.021	81 ± 1
8043961 ¹	0.63	1.559	478.0 ± 10.4	0.000 ± 0.005	184 ± 2
8145477	0.88	0.566	353.7 ± 46.7	0.418 ± 0.007	136 ± 12
8190491	0.95	0.778	594.7 ± 11.7	0.000 ± 0.003	130 ± 1
8211618	0.73	0.337	127.3 ± 66.7	0.319 ± 0.137	31 ± 10
8330092	0.80	0.322	595.5 ± 5.4	0.201 ± 0.001	127 ± 1
8386865 ¹	0.99	1.258	293.9 ± 2.8	0.493 ± 0.013	197 ± 1
8394040 ¹	0.77	0.302	392.6 ± 0.8	0.467 ± 0.001	278 ± 1
8904448 ¹	0.74	0.866	538.8 ± 59.9	0.577 ± 0.016	166 ± 12
9075704	0.68	0.513	396.3 ± 7.5	0.101 ± 0.003	138 ± 1
9451096 ¹	0.54	1.250	106.8 ± 0.1	0.091 ± 0.033	93 ± 1
9706078	0.55	0.614	639.2 ± 27.6	0.550 ± 0.004	237 ± 6
9722737 ¹	0.78	0.419	451.3 ± 3.7	0.152 ± 0.003	225 ± 1
9994475	0.76	0.318	610.9 ± 6.8	0.375 ± 0.001	196 ± 1
10014830 ⁴	0.61	3.031	625.0 ± 44.6	0.487 ± 0.012	156 ± 7
10855535 ⁴	0.98	0.113	411.8 ± 0.5	0.095 ± 0.001	142 ± 1
10991989 ¹	0.54	0.974	554.8 ± 64.1	0.000 ± 0.018	232 ± 17
11247386	0.75	0.394	71.2 ± 0.1	0.217 ± 0.011	38 ± 1
2302092	0.89	0.295	1010.7 ± 48.7	0.468 ± 0.002	435 ± 13
2450566	0.98	1.845	983.7 ± 472.8	0.308 ± 0.016	431 ± 138
2835289 ⁵	0.94	0.858	747.4 ± 23.7	0.643 ± 0.003	338 ± 7

Table 4—Continued

KIC	morph _{bin}	P_{bin} (d)	P_3 (d)	e_3	$A_{LTTE}(s)$
3839964	0.78	0.256	798.2 ± 167.5	0.530 ± 0.016	51 ± 7
4069063 ⁴	0.56	0.504	906.3 ± 26.2	0.516 ± 0.002	430 ± 8
4138301	0.90	0.253	934.1 ± 65.3	0.272 ± 0.002	329 ± 15
4244929	0.91	0.341	1103.1 ± 38.5	0.619 ± 0.001	228 ± 5
4451148	0.82	0.736	746.0 ± 52.1	0.293 ± 0.004	322 ± 14
4547308	0.88	0.577	908.6 ± 75.3	0.000 ± 0.003	154 ± 8
4647652 ¹	0.68	1.065	755.2 ± 44.3	0.244 ± 0.003	239 ± 9
4670267	0.60	2.006	1017.4 ± 429.9	0.751 ± 0.011	82 ± 23
4681152	0.55	1.836	1063.2 ± 510.0	0.514 ± 0.018	88 ± 28
4762887	0.95	0.737	1340.6 ± 849.3	0.000 ± 0.005	52 ± 22
4859432	0.76	0.385	749.6 ± 12.9	0.591 ± 0.001	154 ± 1
4937217	0.82	0.429	1152.6 ± 490.9	0.368 ± 0.013	26 ± 7
4945857	0.74	0.335	1026.6 ± 66.7	0.000 ± 0.002	578 ± 25
5269407	0.53	0.959	1003.2 ± 114.3	0.000 ± 0.003	217 ± 16
5478466	0.97	0.483	934.5 ± 98.2	0.754 ± 0.002	262 ± 18
5611561	0.74	0.259	1033.8 ± 265.3	0.000 ± 0.005	103 ± 17
5790912	0.77	0.383	1245.9 ± 798.3	0.677 ± 0.009	64 ± 27
5791886	0.76	0.325	1032.2 ± 63.0	0.937 ± 0.007	69 ± 2
5975712	0.87	1.136	1164.7 ± 964.3	0.000 ± 0.013	424 ± 234
6050116	0.77	0.240	1078.4 ± 399.2	0.000 ± 0.009	53 ± 13
6118779	0.90	0.364	1281.4 ± 49.4	0.972 ± 0.003	235 ± 6
6281103	0.98	0.363	1018.6 ± 40.5	0.153 ± 0.001	132 ± 3
6469946	0.51	0.716	1246.5 ± 518.1	0.978 ± 0.005	1803 ± 499
6516874	0.60	0.916	857.9 ± 376.5	0.000 ± 0.016	194 ± 56
6543674 ^{3 5}	0.53	2.391	1085.3 ± 224.9	0.593 ± 0.008	263 ± 36
6615041	0.75	0.340	1077.5 ± 42.4	0.107 ± 0.001	68 ± 1
6629588 ⁴	0.55	2.264	818.7 ± 93.5	0.424 ± 0.006	128 ± 9
6671698	0.73	0.472	1048.0 ± 63.2	0.105 ± 0.002	193 ± 7
6766325	0.92	0.440	1316.6 ± 921.7	0.592 ± 0.007	138 ± 64
7035139	0.79	0.310	831.5 ± 38.1	0.479 ± 0.002	62 ± 1
7119757	0.64	0.743	1109.4 ± 398.5	0.666 ± 0.006	427 ± 102
7272739	0.75	0.281	1220.8 ± 354.0	0.554 ± 0.006	83 ± 16
7385478	0.54	1.655	1389.3 ± 795.2	0.245 ± 0.007	243 ± 93
7518816	0.65	0.467	1283.9 ± 618.5	0.481 ± 0.001	73 ± 23
7877062	0.81	0.304	1024.4 ± 31.0	0.169 ± 0.001	93 ± 1
8045121	0.99	0.263	938.6 ± 25.8	0.000 ± 0.001	298 ± 5
8192840 ¹	0.95	0.434	1045.9 ± 185.0	0.616 ± 0.002	260 ± 30
8242493	0.73	0.283	993.5 ± 101.0	0.000 ± 0.003	65 ± 4

Table 4—Continued

KIC	morph _{bin}	P_{bin} (d)	P_3 (d)	e_3	$A_{LTTE}(s)$
8563964	1.00	0.338	1035.2 ± 49.7	0.000 ± 0.001	195 ± 6
8690104	0.77	0.409	1304.2 ± 408.9	0.811 ± 0.009	77 ± 16
8739802	0.93	0.275	869.9 ± 19.9	0.302 ± 0.001	125 ± 1
8957887	0.76	0.347	773.1 ± 12.5	0.561 ± 0.001	401 ± 4
8982514	0.84	0.414	1106.3 ± 61.1	0.000 ± 0.001	58 ± 2
9091810	0.69	0.480	888.9 ± 55.4	0.000 ± 0.003	75 ± 3
9101279	0.58	1.811	1010.9 ± 1000.2	0.212 ± 0.021	78 ± 51
9272276	0.78	0.281	1187.3 ± 133.6	0.347 ± 0.001	458 ± 34
9283826	0.84	0.357	1334.5 ± 381.1	0.000 ± 0.002	169 ± 32
9353234	0.86	1.487	983.9 ± 352.2	0.114 ± 0.010	132 ± 31
9412114	0.85	0.250	1060.9 ± 1527.5	0.330 ± 0.005	450 ± 432
9532219	0.74	0.198	1062.1 ± 76.3	0.372 ± 0.002	70 ± 3
9592145	0.65	0.489	748.7 ± 1091.9	0.396 ± 0.086	14 ± 14
9612468	1.00	0.133	1264.2 ± 233.2	0.340 ± 0.001	118 ± 14
9665086 ⁵	0.67	0.297	882.3 ± 36.9	0.447 ± 0.002	576 ± 16
9821923	0.95	0.350	1295.2 ± 354.8	0.615 ± 0.004	216 ± 39
9838047	0.84	0.436	1082.2 ± 40.7	0.353 ± 0.001	490 ± 12
9912977 ¹	0.59	1.888	780.4 ± 95.2	0.504 ± 0.008	96 ± 7
10226388 ¹	0.77	0.661	965.3 ± 183.8	0.041 ± 0.007	457 ± 58
10275197	0.78	0.391	1093.6 ± 28.5	0.516 ± 0.001	278 ± 4
10322582	0.86	0.291	1362.9 ± 349.1	0.697 ± 0.003	354 ± 60
10383620	0.64	0.735	1111.3 ± 253.4	0.000 ± 0.007	457 ± 69
10388897	0.99	0.344	1367.6 ± 1366.9	0.586 ± 0.005	301 ± 200
10724533	0.75	0.745	1131.4 ± 197.7	0.265 ± 0.003	73 ± 8
10727655	0.73	0.353	1087.9 ± 67.6	0.000 ± 0.001	309 ± 12
10848807	0.74	0.346	799.1 ± 135.4	0.430 ± 0.011	31 ± 3
10905804	0.68	0.751	1154.1 ± 471.0	0.484 ± 0.022	49 ± 13
10916675	0.87	0.419	1170.9 ± 244.5	0.609 ± 0.007	29 ± 4
10934755	0.68	0.786	1021.3 ± 112.6	0.302 ± 0.005	84 ± 6
11042923 ¹	0.76	0.390	984.4 ± 63.9	0.258 ± 0.002	276 ± 11
11246163	0.77	0.279	1010.6 ± 181.3	0.164 ± 0.005	69 ± 8
11347875	0.86	3.455	1180.4 ± 547.1	0.000 ± 0.011	453 ± 140
11604958	0.72	0.299	1068.9 ± 229.6	0.000 ± 0.006	41 ± 5
11716688	0.94	0.301	1371.3 ± 2011.1	0.477 ± 0.004	462 ± 452
11825204	0.98	0.210	1336.0 ± 1253.8	0.414 ± 0.004	682 ± 426
12019674	0.76	0.355	1088.4 ± 34.7	0.346 ± 0.001	198 ± 4
12055255	0.90	0.221	1093.4 ± 22.6	0.479 ± 0.001	297 ± 4
12071741	0.94	0.314	939.0 ± 78.6	0.737 ± 0.002	473 ± 26

Table 4—Continued

KIC	morph _{bin}	P_{bin} (d)	P_3 (d)	e_3	$A_{LTTE}(s)$
12458133	0.76	0.333	1116.4 ± 396.0	0.484 ± 0.012	25 ± 6
3114667	0.52	0.889	~ 500
2983113	0.89	0.395	~ 1300
4066203	0.93	0.363	~ 700
4074708	0.73	0.302	~ 1100
4904304	0.89	0.389	~ 1300
5282464	0.72	0.496	~ 1100
5956776	0.61	0.569	~ 700
6153219	0.62	0.530	~ 700
6265720	0.92	0.312	~ 1300
6794131	0.81	1.613	~ 1300
7506164	0.88	0.558	~ 1300
7590728	0.69	0.477	~ 900
9544350	0.92	2.260	~ 1000
9776718	0.87	0.544	~ 800
9788457	0.60	0.963	~ 1000
10095469	0.60	0.678	~ 800
10796477	0.74	0.485	~ 1100
2159783	0.87	0.374	~ 1900
3127873	0.91	0.672	~ 4200
3221207	0.81	0.474	~ 1700
3342425	0.93	0.393	~ 6200
3766353	0.53	2.667	~ 6100
3848042	0.99	0.411	~ 2600
3935319	0.75	0.353	~ 1400
3936357 ⁴	0.76	0.369	~ 2400
4077442	0.58	0.693	~ 6900
4464999	0.77	0.434	~ 3000
4563150	0.79	0.275	~ 2000
4758368	0.57	3.750	~ 1500
4945588	0.99	1.129	~ 1500
5008287	0.94	0.292	~ 2300
5015926	0.75	0.363	~ 1400
5097446	0.60	1.288	~ 6100
5296877	0.95	0.377	~ 1900
5353374	0.78	0.393	~ 1700
5389616	0.99	0.407	~ 2100
5513861 ²	0.57	1.510	~ 1800

Table 4—Continued

KIC	morph _{bin}	P_{bin} (d)	P_3 (d)	e_3	$A_{LTTE}(s)$
5770431	0.89	0.392	~ 4900
5820209	0.81	0.656	~ 1600
5951553	0.95	0.432	~ 2300
6144827	0.79	0.235	~ 5000
6187893	0.59	0.789	~ 7800
6287172	0.95	0.204	~ 1400
6370361	0.84	0.455	~ 6200
7137798	0.51	2.254	~ 6700
7269843	0.79	0.268	~ 6200
7339345	0.74	0.260	~ 2500
7367833	0.76	0.286	~ 2200
7375612 ⁴	0.97	0.160	~ 2100
7680593	0.97	0.276	~ 1500
7697065	0.69	0.273	~ 2100
7709086	0.78	0.409	~ 2000
7773380	0.94	0.308	~ 1400
7871200	0.74	0.243	~ 6800
7878402	0.73	0.374	~ 7700
8016214	0.53	3.175	~ 2100
8122124 ⁴	1.00	0.249	~ 1600
8189196	0.98	2.304	~ 8300
8222945	0.99	0.451	~ 2300
8231231	0.89	0.712	~ 1600
8257903	0.76	0.515	~ 4100
8265951	0.81	0.780	~ 2000
8703528	0.74	0.400	~ 1500
8715667	0.85	0.406	~ 6200
8758716 ⁴	1.00	0.107	~ 4900
9026766	0.75	0.272	~ 8900
9083523	0.65	0.918	~ 5200
9097798	0.99	0.334	~ 4000
9181877	0.74	0.321	~ 2600
9347868	0.82	0.318	~ 9500
9657096	0.94	2.138	~ 1400
9724080	0.94	1.174	~ 3000
9882280	0.75	0.289	~ 3100
9956124	0.91	0.363	~ 8800
10007533	0.88	0.648	~ 5600

Table 4—Continued

KIC	morph _{bin}	P_{bin} (d)	P_3 (d)	e_3	$A_{LTTE}(s)$
10135584	0.96	0.391	~ 4200
10216186	0.64	0.606	~ 5400
10228991	0.97	2.799	~ 1600
10229723	0.83	0.629	~ 7400
10481912	0.96	0.442	~ 2700
10485137	0.71	0.445	~ 3100
10557008	0.77	0.265	~ 1500
10711938	0.95	0.358	~ 2000
11091082	0.82	0.385	~ 1400
11151970	0.87	0.312	~ 9000
11305087	0.78	0.309	~ 5300
11496078	0.87	0.300	~ 6500
11509282	0.83	0.634	~ 1600
11566174	0.76	0.277	~ 3200
11717798	0.83	0.375	~ 8000
11805235	0.79	0.395	~ 5400
11910076	0.96	0.348	~ 4600
12055421	0.96	0.386	~ 1600
12267718	0.89	0.545	~ 7000
12554536	0.63	0.684	~ 2200

Note. — This table is divided into three sections based on the period for the third body found by the LTTE fit. The first section includes periods from 0-700 days (approximately half the length of the time-baseline of the photometric data used), the second from 700-1400 days (approximately the length of the time baseline), and the third longer than 1400 days. In the first section, the fits are based on at least 2 full cycles of the LTTE orbit, the second on 1 full cycle, and the third is a very preliminary fit based on some evidence of curvature in the ETVs. Some binaries with third body signals that fell in the second section did not have *Kepler* data available for the full baseline. These no longer met the criteria of having a full cycle of data, and so were moved to the beginning of the third section of the table. These three different sections are noted in all plots with black, gray, and light gray respectively.

¹Appears in Rappaport et al. (2013)

²Appears in Gies et al. (2012) as candidate third-body

³Slawson et al. (2011)

⁴Shows depth variations

⁵Visible tertiary eclipse